Materials Today Bio 30 (2025) 101408

Contents lists available at ScienceDirect

Materials Today Bio

journal homepage: www.journals.elsevier.com/materials-today-bio

The immunoglobulin of yolk and cerium oxide-based fibrous poly (L-lactide-co-glycolide)/gelatin dressings enable skin regeneration in an infectious wound model

Xinyuan Zhao [a,1], Changwen Weng [b,1], Hao Feng [c], Muhammad Shafiq [d], Xinyi Wang [c], Lei Liu [b], Lu Han [c], Mohamed EL-Newehy [e], Meera Moydeen Abdulhameed [e], Zhengchao Yuan [c,**], Xiumei Mo [c,*], Yanbiao Wang [f,***]

[a] Shandong First Medical University & Shandong Academy of Medical Sciences, Jinan 250117 Shandong, China
[b] Department of Hernia and Abdominal Wall Surgery, Shanghai East Hospital, TongJi University, 150 Ji Mo Road, Shanghai 200120, PR China
[c] State Key Laboratory for Modification of Chemical Fibers and Polymer Materials, Shanghai Engineering Research Center of Nano-Biomaterials and Regenerative Medicine, College of Biological Science and Medical Engineering, Donghua University, 201620, Shanghai, China
[d] Innovation Center of NanoMedicine (iCONM), Kawasaki Institute of Industrial Promotion, Kawasaki-ku, Kawasaki 210-0821, Japan
[e] Department of Chemistry, College of Science, King Saud University, P.O. Box 2455, Riyadh 11451, Saudi Arabia
[f] Department of Orthopedics, the Third Affiliated Hospital of Shandong First Medical University (Affiliated Hospital of Shandong Academy of Medical Sciences), NO.38, Wuyingshan Road, Tianqiao District, Jinan 250031, PR China

ARTICLE INFO

Keywords:
Cerium oxide nanoparticles
Immunoglobulin of yolk
Electrospinning
Nanofiber membrane
Wound healing

ABSTRACT

The bacterial infection and oxidative wound microenvironment delay skin repair and necessitate intelligent wound dressings to enable scarless wound healing. The immunoglobulin of yolk (IgY) exhibits immunotherapeutic potential for the potential treatment of antimicrobial-resistant pathogens, while cerium oxide nanoparticles (CeO_2 NPs) could scavenge superoxide dismutase (SOD) and inflammation. The overarching objective of this study was to incorporate IgY and CeO_2 NPs into poly(L-lactide-co-glycolide)/gelatin (PLGA/Gel)-based dressings (P/G@IYCe) for infected skin repair. The P/G@IYCe manifested good biocompatibility as well as showed significant antibacterial effect against Staphylococcus aureus (*S. aureus*) and Escherichia coli (*E.coil*) *in vitro*. Subcutaneous implantation of membranes in rats exhibited cytocompatibility. Transplantation of membranes in *S. aureus*-infected full-thickness excisional defects manifested significant beneficial effect of P/G@IYCe dressings than that of the other groups in terms of the scar tissue formation, inflammation resolution, and scavenging of reactive oxygen species (ROS) at 2 weeks post-transplantation. Taken together, the dual delivery of IgY and CeO_2 may enable intelligent wound dressings.

1. Introduction

Antibiotics are widely used to treat bacterial infections albeit risks associated with their overuse, such as antibiotic resistance [1,2]. Functional inorganic nanomaterials, including silver and zinc oxide (ZnO) possess antibacterial effect and are widely used as an alternative therapeutic options for infection management, thanks to their ability to disrupt cellular membrane as well as disintegrate bacterial biofilm [3,4]. Despite advantageous features of inorganic nanomaterials, their widespread utilization is mainly hindered owing to their potential cytotoxicity and biological safety [5,6]. Cerium oxide (CeO_2) NPs have also been utilized for regenerative medicine and tissue engineering (TE) applications and shown to promote blood vessel formation and scavenge reactive oxygen species (ROS), which may have implications for the skin repair [7]. However, the utilization of CeO_2 NPs into dressings is confronted with several persisting challenges, including an uncontrollable release, potential cytotoxicity, and biological safety [8]. While functional nanomaterials are appealing therapeutic options for the infected

* Corresponding author.
** Corresponding author.
*** Corresponding author.
E-mail addresses: yuanzhengchao2021@163.com (Z. Yuan), xmm@dhu.edu.cn (X. Mo), drwangyanbiao@163.com (Y. Wang).
[1] X. Zhao and C. Weng are co-first authors.

https://doi.org/10.1016/j.mtbio.2024.101408
Received 12 October 2024; Received in revised form 8 December 2024; Accepted 15 December 2024
Available online 17 December 2024

skin regeneration, natural bioactive materials also play a vital role to promote tissue regeneration [5].

Chicken egg yolk immunoglobulins (IgY) derived from immunized chickens lacks immunological cross-reactivity unlike mammalian immunoglobulin G (IgG), resolves inflammatory response, and does not activate complement system [9]. The IgY has been used as a viable source for polyclonal antibodies [9,10]. The IgY antibodies may perturb bacterial infection and bacterial biofilm formation via different mechanisms, such as binding with the adhesion/virulence molecules of the targets of surviving bacteria and coating of the whole bacterial cell wall, thereby constricting bacterial growth [11]. Thus, the passive immunization with IgY is an efficient approach for the treatment of drug-resistant pathogens [12]. Since infected wounds pose an overwhelming therapeutic challenge worldwide, the utilization of IgY into wound dressings may offer a promising platform for the treatment of infected skin repair as well as help manage bacterial biofilms due to drug-resistant bacterial species [13–15]. Moreover, the wound healing requires blood vessel regeneration, inflammation resolution, and timely scavenging of oxidative species [16,17]. Similar to inorganic nanoparticles (NPs), such as CeO_2, IgY lacks an appropriate application form to harness its therapeutic effects for skin repair, and therefore necessitates an advent of alternative platforms for its sustained and controlled release [18,19].

Tissue-engineered scaffolds, such as hydrogels, aerogels and fibers, may be exploited to achieve the sustained and controlled release of IgY and CeO_2 NPs [20]. The scaffolds can promote the wound healing process by involving the coordinated activity of different cell types, biological components, and bio-materials [7]. Electrospun fibers exhibit extracellular matrix (ECM)-mimetic morphology, and have been shown to facilitate cell proliferation, cell migration, and cell differentiation [21]. Moreover, electrospun fibers possess advantageous physical and chemical features, including nano-scale pore size, large surface area-to-volume ratio, which could be utilized to encapsulate therapeutics, biologics, and bioactive cues [20]. Besides, dressings composed of electrospun fibers can isolate the wound site from the external environment and confer a moist environment at the wound site, thereby serving as promising candidates for skin repair [20]. We envisioned that the electrospun fibers may enable the successful incorporation of IgY and CeO_2 NPs into dressings as well as afford sustained release of bioactive components, and avoid potential toxicity associated with the high concentrations in the wound tissue site [22].

In this study, we focussed on the incorporation of IgY and CeO_2 NPs into electrospun fibers-based dressings and investigated antibacterial, anti-inflammatory, and ROS scavenging ability of dressings *in vitro* and *in vivo*. We performed a series of *in vitro* and *in vivo* assays to delineate the regulatory effect of IgY and CeO_2 NPs for ROS scavenging, inflammatory response, and antibacterial activity. We additionally delineated the beneficial effect of the bioactive components to enable scarless tissue repair in an infectious wound healing model in rats. The P/G@IYCe fibers were shown to suppress bacterial adhesion and growth, scavenge ROS, resolve inflammatory response, and promote infectious wound tissue repair, which may have broad implication for skin repair and potentially other bio-related applications.

2. Experimental

2.1. Materials

The IgY was purchased from the Shandong Beirikang Biotechnology Co., Ltd (Weifang, China). Poly(L-lactide-co-glycolide) (PLGA, *M*n = 70–110 kDa) and gelatin Type B (Gel, 48722-500G-F) were respectively obtained from Jinan Daigang Bioengineering Co., Ltd. (Jinan, China) and MP Biomedicals, LLC (Shanghai, China). Cerium oxide NPs (CeO_2; CAS#1306-38-3; Φ = 2–6 nm) were acquired from Nanami XFNANO Materials Tec Corporation (Nanjing, China). Escherichia coli (*E. coli*, ATCC 25922), and Staphylococcus aureus (*S. aureus*, ATCC 25923) were provided by Chinese Academy of Sciences (Shanghai, China). Enzyme-linked immunosorbent assay (ELISA) kit for the IgY was purchased from Shanghai Jichun Industrial Co., Ltd (Shanghai, China, catalog # ml002802).

2.2. Preparation of membranes

To prepare electrospun membrane, PLGA and Gel were dissolved using 1,1,1,3,3,3- hexafluoro-2-propanol (HFIP) to afford 10 % (w/v) solution (PLGA:Gel = 7/3, w/w) and represented as P/G. Thereafter, 200 mg of IgY and 100 μL of CeO_2 NPs solution were respectively added into 10 of mL P/G solution to prepare P/G@IY and P/G@Ce solution. For the fabrication of P/G@IYCe, 200 mg IgY and 100 μL of CeO_2 solution were added into 10 of mL P/G solution. Electrospun membranes were fabricated using a commercial electrospinning setup (Yongkang Leye Technology Development Co., Ltd. SS-3556H, Beijing, China) with following electrospinning parameters: applied voltage, 12 kV, flow rate, 1.5 mL/h, and electrospinning time, 3 h. The obtained scaffolds were stored at 4 °C.

2.3. Physicochemical characterization

Scanning electron microscopy (SEM, Hitachi, TM-1000, Tokyo, Japan) was used to observe the morphology of fibers, while energy-dispersive X-ray spectroscopy (EDS) was used for the elemental mapping of fibrous membrane. The CFP-1100-AI capillary flow porometer (PMI Porous Materials Inc., Ithaca, NY, USA) was used to analyze the pore size distribution of P/G@IYCe scaffolds (thickness = 0.30–0.35 mm; Φ, 30 mm).

To discern the release kinetics of IgY, 100 mg of P/G@IY samples were immersed into 25 mL of phosphate-buffered saline (PBS) solution and stirred at 37 °C and 120 rotations per minute (rpm). At predetermined time points, 100 μL of solution was collected and replaced with the fresh solution to realize infinite sink conditions. The concentration of the IgY was analyzed using IgY ELISA assay kit following manufacturer's instructions. For water absorption and mechanical properties, the detailed procedures are described in Supplementary Information.

2.4. Biocompatibility and biological functions of membranes in vitro

2.4.1. Biocompatibility

Hemocompatibility of membranes was assessed using fresh rabbit blood, while cytocompatibility was studied using human umbilical vein endothelial cells (HUVECs) and NIH-3T3 fibroblasts with CCK-8 assay, live/dead staining, and F-actin/DAPI staining. The detailed methods are described in the supporting information.

2.4.2. Transwell migration and scratch wound healing assay

Cell migration was studied using Transwell migration assay and scratch wounding assay *in vitro* (see supporting information for the procedure).

2.4.3. Antibacterial activity

The *S. aures* and *E. coil* were used to discern the antibacterial performance of membranes. Briefly, the samples (thickness, 0.30–0.35 mm; Φ, 10 mm) and 1 mL of bacterial culture solution (1×10^5 CFU/mL) were added into a 24-well plate for incubation at 37 °C for 24 h. Thereafter, solution was transferred to 10 mL of PBS, seeded on agar plate and incubated at 37 °C for 24 h. Finally, the bacterial colonies were photographed and the quantitatively analysis was performed by image J (NIH, v1.8.0, USA).

2.5. Animal experiments

2.5.1. Subcutaneous implantation of membranes in vivo

Animal procedures received approval from the Animal Care Committee of Donghua University, Shanghai, China (approval # DWSY202409100091). For preliminary assessment of the biocompatibility of membranes, samples (thickness, 0.30–0.35 mm; 5 mm × 5 mm) were subcutaneously implanted in Sprague-Dawley (SD) rats for up to 3 weeks. Animals were anesthetized by using an intraperitoneal injection of 3 % sodium pentobarbital and subcutaneous pocket was created for the implantation of membranes. At week 1, 2, and 3, animals were sacrificed with an overdose of intraperitoneal injection of sodium pentobarbital, and the scaffolds along with their adjacent tissues were explanted. For cell infiltration and collagen regeneration, explanted samples were stained by the Hematoxylin and Eosin (H&E) and Masson's trichrome (MT) staining.

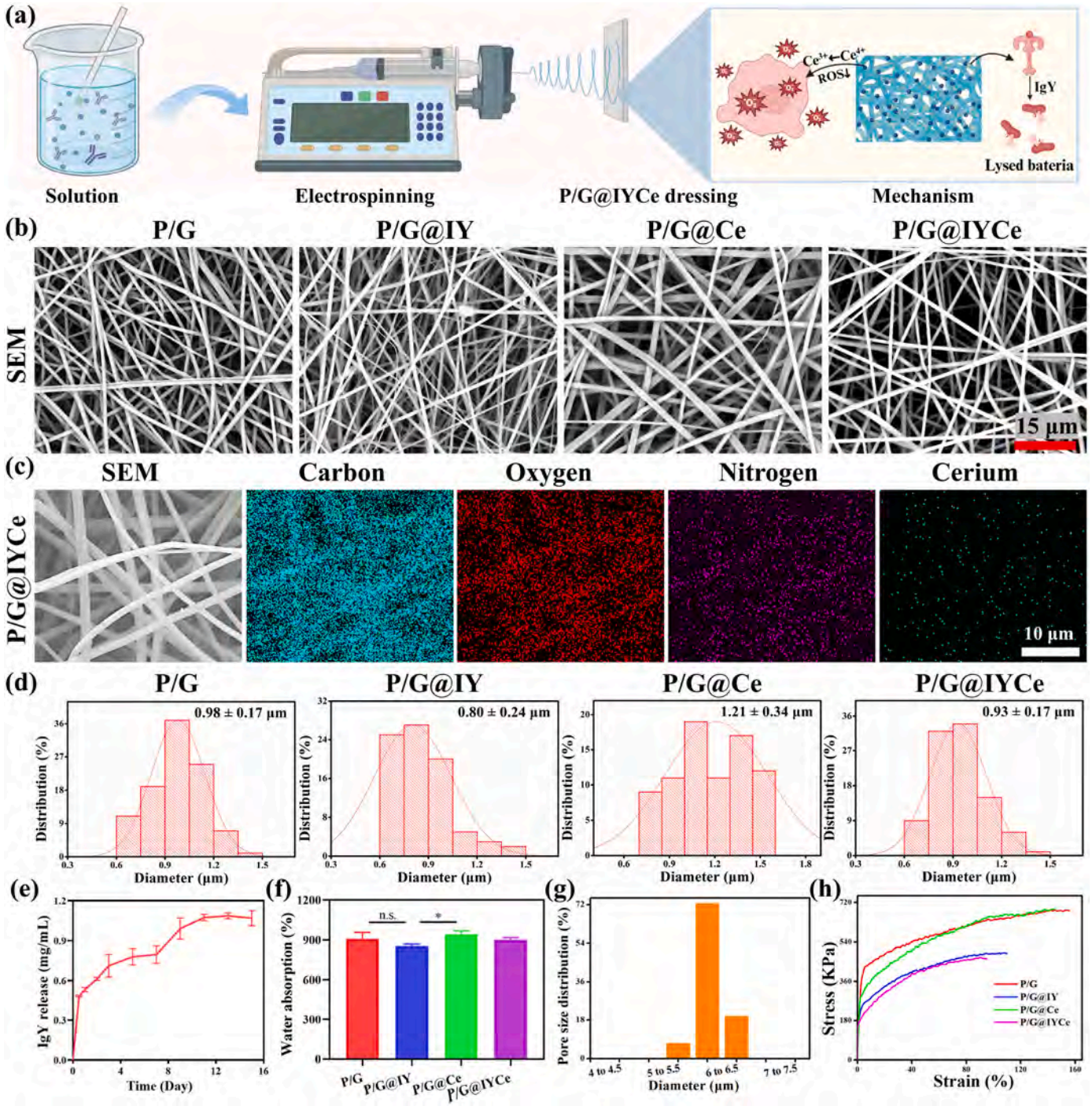

Fig. 1. Morphological analysis of membranes, EDS analysis, and size distribution. (a) Schematic diagram showing the synthesis scheme of P/G@IYCe membrane. (b) SEM images of scaffolds. (c) EDS analysis. (d) Average fiber diameter distribution. Scale bar: 10 μm (c). The cumulative release of IgY from the P/G@IYCe scaffolds (e). The pore size distribution of P/G@IYCe scaffolds (f). The maximum water absorption (g) and strain-stress curve (h) for P/G, P/G@IY, P/G@Ce, and P/G@IYCe groups.

2.5.2. Wound healing efficacy of membranes in vivo

For wound healing assay, the 6-week-old of SD rats were randomly divided into six groups (n = 3) to receive different types of samples (control, sterile gauze; positive control, biocellulose-based dressings; P/G; P/G@IY; P/G@Ce; and P/G@IYCe). Briefly, rats were anesthetized, and full-thickness excisional defects (Φ = 10 mm) were created. For bacteria-infected wound model, defects were administered with 20 μL of *S. aureus* suspension (10^7 colony forming units (CFU)) and were covered with the dressings for up to 14 days. Digital images of wounds were collected and wound healing was delineated at day 0, 3, 7, 10, and 14 for all groups. H&E staining and MT staining were carried out following routine histological analysis methods. For antioxidative properties, immunofluorescence (IF) staining for ROS was performed at day 14.

The bacterial activity of wound site was assayed at day 7 post-implantation. Briefly, 100 μL of normal saline was added into the wound site to collect the residual bacteria and dry cotton gauze was used to absorb the wound exudate. Finally, the cotton gauze alongside the bacterial microorganisms was transferred into the LB liquid medium (10 mL), and the solution (100 μL) was seeded on the agar plate at 37 °C for 24 h to analyze the colony growth.

2.6. Statistical analysis

All experiments were carried out with at least three samples, and data were showed means ± standard error. Statistical differences among more than two groups were calculated using one-way ANOVA with Tukey's test. Significant difference was recorded as significant when $p < 0.05$ (*), $p < 0.01$ (**), $p < 0.001$ (***).

3. Results

3.1. Characterizations

Electrospinning has been widely used to prepare scaffolds for regenerative medicine and TE applications (Fig. 1a) [18]. Electrospun fibers exhibit ECM-mimetic morphological features [22]. SEM micrographs showed the morphology of different membranes, including P/G, P/G@IY, P/G@Ce, and P/G@IYCe (Fig. 1b). The fibers displayed a smooth surface morphology with bead formation (Fig. 1b). The average diameter of the fibers was 0.98 ± 0.17 μm, 0.80 ± 0.24 μm, 1.21 ± 0.34 μm, and 0.93 ± 0.17 μm for P/G, P/G@IY, P/G@Ce, and P/G@IYCe groups, respectively (Fig. 1d). The EDS mapping of the P/G@IYCe membranes further indicated the distribution of various elements, including carbon, oxygen, nitrogen, and cerium (Ce). On the other hand, P/G and P/G@IY membranes did not show the Ce element. These data showed that the CeO_2 NPs were successfully loaded into P/G@IYCe fibers and were homogenously distributed (Fig. 1c, Fig. S1).

We next elucidated the release of IgY from membranes. The concentration of the IgY released from P/G@IYCe membranes was found to be 0.71 ± 0.08 mg/mL and 1.07 ± 0.06 mg/mL at day 3 and day 11, respectively (Fig. 1e– S2). The water absorption rate of P/G, P/G@IY, P/G@Ce, and P/G@IYCe scaffolds was 908.2 ± 50.0 %, 855.4 ± 14.9 %, 942.6 ± 27.1 %, and 903.0 ± 15.4 %, respectively (Fig. 1f). Since dressings exhibited significant water uptake, they may absorb tissue exudate at the wound site. The pore size distribution of membranes was varied in range from 4.9 μm to 6.5 μm, while the average pore size was 5.81 μm, which may have implications for the diffusion of oxygen from the fibers (Fig. 1h).

Moreover, the stress-strain curves indicated that the scaffolds showed the Hooke's law in the initial stage followed by the plastic deformation beyond the yield point (Fig. 1h). The tensile strength was 763.3 ± 111.0 kPa, 499.1 ± 111.0 kPa, 751.4 ± 56.5 kPa, 481.9 ± 46.1 kPa for P/G, P/G@IY, P/G@Ce, and P/G@IYCe groups, respectively. These results indicated that while CeO_2 NPs did not significantly affect the mechanical behavior of membranes, IgY may reduce the mechanical behavior, such as the tensile strength (TS) due to its rapid dissolution properties (Fig. S3).

3.2. Biocompatibility and biofunction assay in vitro

Since wound dresings can interact with the blood at the injury site, it is imperative to discern the hemocompatibility of membranes by measuring the amount of the ruptured erythrocytes in contact with the scaffolds [20]. We therefore evaluated the biocompatibility of membranes *in vitro*. The positive control group exhibited bright red colour of the supernatant indicating the disrupted erythrocytes and the potential release of the hemoglobin from RBCs (Fig. 2a). However, the supernatants in P/G, P/G@IY, P/G@Ce, and P/G@IYCe groups displayed slight yellowish colour mirroring colorless suspension of the negative control, thereby indicating intact erythrocytes (Fig. 2a). The hemolysis ratio was less than 5 % in all scaffolds (0.57 ± 0.12 %, 0.56 ± 0.40 %, 0.83 ± 0.11 %, and 1.00 ± 0.45 % for P/G, P/G@IY, P/G@Ce, and P/G@IYCe groups, respectively), which is indicative of the good hemocompatibility of scaffolds (Fig. 2e).

The preliminary biocompatibility of the wound dressings was evaluated by culturing cells along with the extract solution obtained from the dressings. The extract solution of various groups was cytocompatibility and non-cytotoxic as revealed by culturing HUVECs and NIH-3T3 fibroblast along with the extract solution for up to 5 days *in vitro* (Fig. 2f and g). The P/G@Ce and P/G@IYCe groups exhibited the highest cell vitality and possessed more number of viable cells for both cell types at day 5 as compared to the other groups, such as P/G and P/G@IY (Fig. 2b and c). The cytoskeletal organization of HUVECs was assessed by staining the cell cultures with Filamentous actin (F-actin) and 4′,6-diamidino-2-phenylindole (DAPI) staining. The HUVECs cultured along with the extract solution of the P/G@IY, P/G@Ce, and P/G@IYCe manifested pseudopodia, which is indicative of their good spreading (Fig. 2d).

Wound healing triggers the mobilization and recruitment of different cell types, including keratinocytes, fibroblasts, endothelial cells (ECs) and stem/progenitor cells; adequate regulation of cell mobilization and recruitment to the injury site may be instrumental to promote the skin repair [23]. Consequently, we employed HUVECs to ascertain the chemotactic potential of different types of dressings *in vitro*. Both the CeO_2 NPs and IgY manifested chemotactic effect and promoted the migration of HUVECs as delineated with a Transwell migration assay *in vitro* (Fig. 3a). The P/G@IY, P/G@Ce, and P/G@IYCe groups showed significantly more number of migrated cells per high power field (HPF) than that of the control and P/G groups (control, 7.7 ± 2.5, P/G, 12.3 ± 3.1, P/G@IY, 15.0 ± 2.0, P/G@Ce, 19.7 ± 1.5, and P/G@IYCe, 25.0 ± 2.0 per hpf) (Fig. 3d). We further delineated the migration of HUVECs using a scratch wounding assay *in vitro*, which also replicated the findings of the Transwell migration assay (Fig. 3b). The scaffolds co-loaded with the IgY and CeO_2 NPs facilitated the cell migration *in vitro* (Fig. 3b and e).

Anti-bacterial performance of dressings was studied using *E. coli* and *S. aureus* (Fig. 3c). The survival ratio of *E. coli* was 100.0 ± 4.6 %, 64.1 ± 6.7 %, 24.6 ± 2.5 %, 33.6 ± 1.5 %, and 12.3 ± 2.0 %, while that of the *S.aures* was 100.0 ± 2.8 %, 91.6 ± 3.9 %, 5.3 ± 0.5 %, 26.5 ± 1.0 %, and 4.7 ± 0.3 % for control, P/G, P/G@IY, P/G@Ce, and P/G@IYCe groups, respectively (Fig. 3f). P/G@IY and P/G@IYCe groups showed significantly less number of bacterial species than that of the other groups, thereby indicating anti-bacterial effect of IgY (Fig. 3c). The P/G@Ce group also showed less number of residual bacterial colonies as compared to the control and P/G groups (Fig. 3c and f).

3.3. Biocompatibility assay in vivo

The preliminary biocompatibility of dressings was evaluated in a subcutaneous implantation model for up to 6 weeks (Fig. 4a). The cell infiltration as well as inflammatory response and neo-tissue formation were delineated by H&E staining. H&E staining of explanted scaffolds

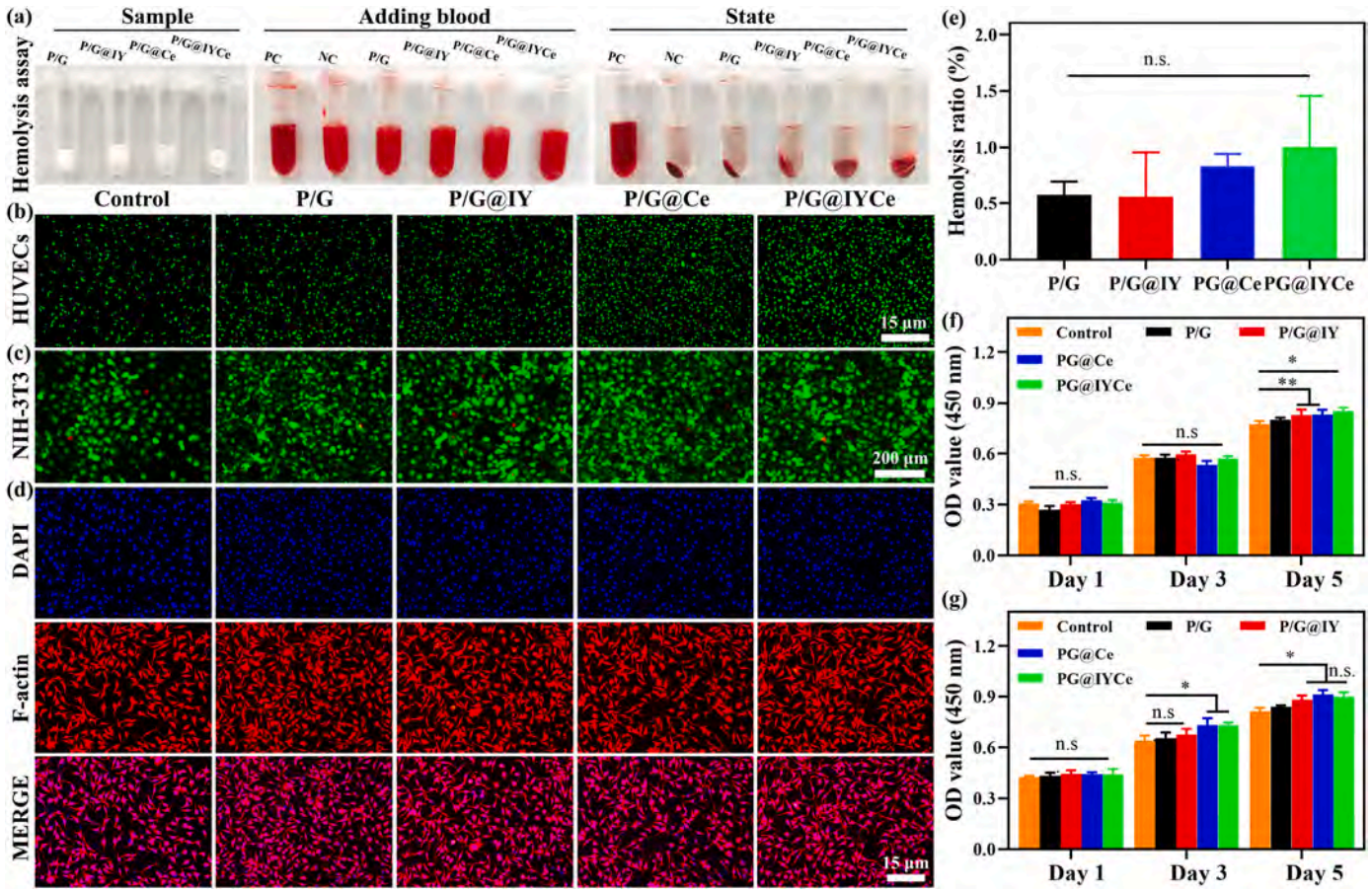

Fig. 2. Hemocompatibility and cytocompatibility assay. (a) The scheme showing the procedure of hemolysis assay. PC (positive group, DI water) and NC (negative control, normal saline) groups. Live/dead staining of HUVECs (b) and NIH-3T3 fibroblast (c) co-cultured along with the extract solution of different samples at day 5. (d) The DAPI and F-actin staining for HUVECs co-cultured with the extract solution of samples at day 5. Quantitative analysis of the hemolysis ratio (e), proliferation of HUVECs (f) and NIH-3T3 fibroblast (g) co-cultured along with the extract solution of various samples for up to day 5.

manifested cellular infiltration as well as inflammatory cell recruitment and the degradation of scaffolds *in vivo* (Fig. 4b–d). Cellularization as well as thickness of the membranes were gradually increased with an increase in the implantation time (Fig. 4b–d). We also quantitatively analyzed the portion of the explanted scaffolds which lacked cellular infiltration. The thickness of the scaffolds lacking infiltrated cells was 158.1 ± 16.7 μm, 151.9 ± 19.6 μm, 150.1 ± 26.2 μm, and 99.3 ± 8.8 μm at 2 weeks, while 416.3 ± 27.4 μm, 624.2 ± 55.9 μm, 438.0 ± 130.5 μm, and 624.9 ± 73.3 μm at 4 weeks post-operatively for P/G, P/G@IY, P/G@Ce, and P/G@IYCe groups, respectively (Fig. 4f and g). These data showed that the host cells can be infiltrated into scaffolds, which even became further pronounced 6 weeks post-operatively.

By week 6, almost the whole thickness of the membranes was accumulated with the host cells as well as collagen tissues in all groups (Fig. 4d). The P/G@IYCe group showed significantly higher degradation and was accompanied by significant accumulation of collagen tissues (Fig. 4e). The thickness of the scaffolds lacking cellular infiltration was found to be 94.2 ± 17.4 μm, 56.8 ± 8.5 μm, and 66.9 ± 8.2 μm for P/G, P/G@IY, and P/G@Ce groups, respectively (Fig. 4h). These results showed that the IgY and CeO_2 NPs can synergistically promote the degradation of the scaffolds alongside significant regeneration of collagen.

3.4. Wound healing assay

Based on the antibacterial potential of IgY and CeO_2 NPs, the healing performance of dressings was assessed in an *S. aureus*-infected full-thickness excisional defect wound model in rats (Fig. 5a). The wound defects treated with P/G@Ce and P/G@IYCe were gradually healed with minimal residual unhealed area (Fig. 5b). In contrast, untreated wounds (control group) and P/G group (P-control) still displayed residual wound defect at day 14 post-operatively (Fig. 5b, 5e-5f). The dressings co-loaded with the IY and CeO_2 promoted significant wound repair than that of the other groups (wound closure percentage: P/G@IYCe, 73.3 ± 3.0 %, P/G@Ce, 46.1 ± 4.6 %, P/G@Ce, 38.4 ± 1.1 % vs. P/G, 33.3 ± 1.7 %, and control, 16.6 ± 2.9 % at day 14) (Fig. 5b and e). The H&E staining exhibited more number of inflammatory cells at the wound site for all groups at day 7 (Fig. 5c). By day 14, the wounds in the P/G@Ce and P/G@IYCe groups exhibited only a few number of inflammatory cells (Fig. 5d). These results indicated that the IgY and CeO_2 can delay the inflammatory response as well as promote skin repair.

MT staining revealed an insignificant epithelial regeneration in all groups for up to day 7, while there was significant epithelial regeneration in P/G@Ce and P/G@IYCe groups at day 14 (Fig. 5c and d). Since epithelium formation is an important indicator of wound healing, it was further analyzed by the H&E staining at day 14 (Fig. 5d). Control and P/G groups lacked intact epithelial layer formation, while other groups manifested intact epithelial layers of varying thickness (Fig. 5d). The thickness of epithelium layer was 39.8 ± 4.9 mm, 72.1 ± 15.0 mm, and 80.4 ± 11.5 mm for P/G, P/G@IY, P/G@IYCe groups, respectively (Fig. 5g). P/G@IYCe group further exhibited negligible scar length as compared to the other groups (scar length: P/G@IYCe, 1.6 ± 0.4 mm, P/G@Ce, 3.0 ± 0.4 mm, P/G@IY, 3.4 ± 0.2 mm, P/G, 2.44 ± 0.3, and control, 4.6 ± 0.4 mm) (Fig. 5h).

To evaluate the antimicrobial function of the dressing *in vivo*, the residual bacteria at wound site was assayed by spread plate method at

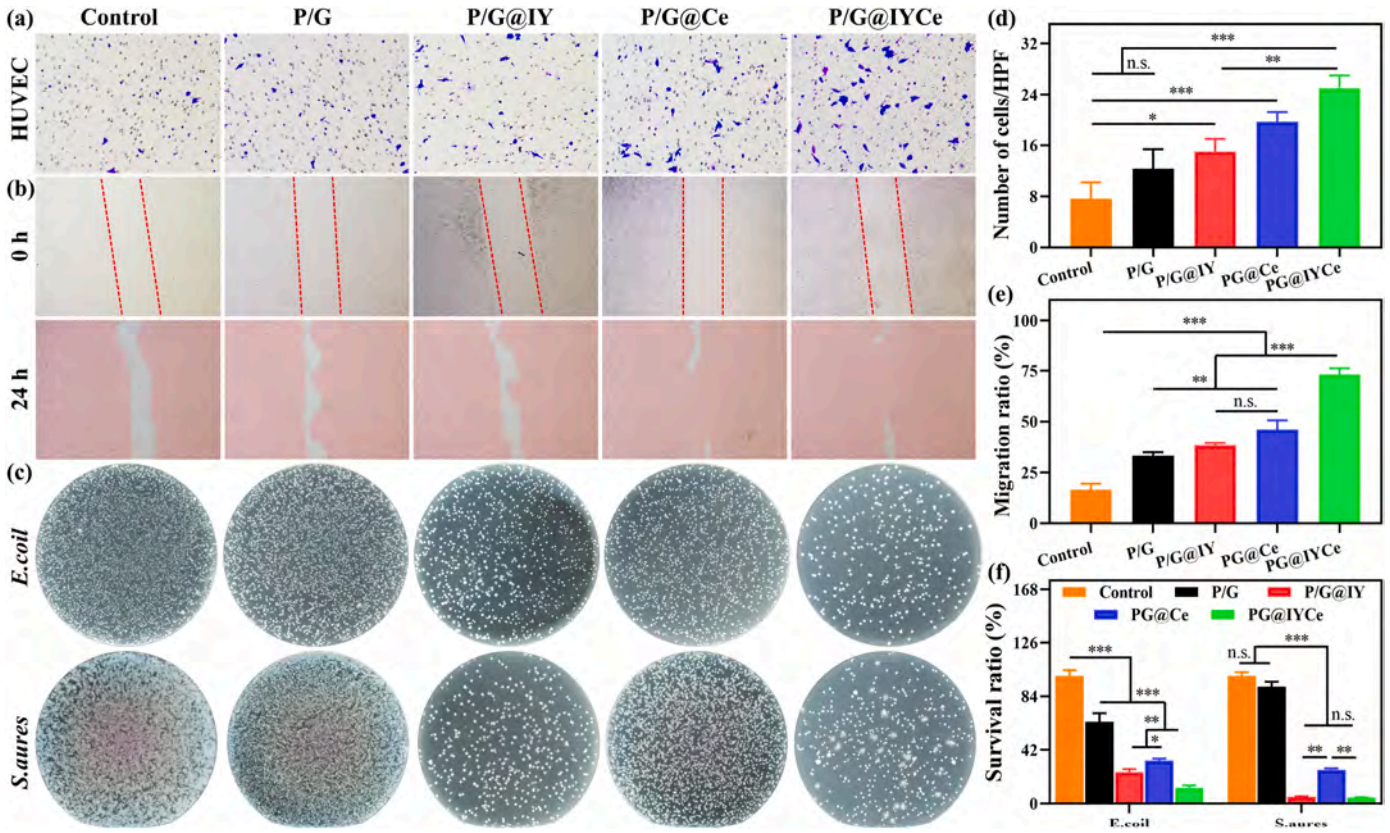

Fig. 3. Biofunction assay *in vitro*. (a) Transwell migration of HUVECs at 12 h, (b) scratch wounding assay of HUVECs at 0 h and 24 h. (c) Growth of *E. coli* and *S. aureus* on broth agar plates after treatment with different types of scaffolds. Quantitative analysis HUVECs migrated in a Transwell migration assay *in vitro* (d) and scratch wound healing assay (e) for control as well as various dressing groups. (f) The survival ratio of *E. coli* and *S. aureus*.

day 7 (Fig. 6a). P/G@Ce and P/G@IYCe groups showed less bacterial colonies than that of other groups, which recapitulated the *in vitro* findings of antibacterial test (Fig. 6b). The survival ratio of bacteria was significantly less in the P/G@Ce and P/G@IYCe groups than that of the other groups at day 7 (residual bacteria at the wound site: P/G@IYCe, 24.6 ± 2.4 %, P/G@Ce, 34.2 ± 2.5 %, P/G@IY, 118.5 ± 4.7 %, P/G, 153.6 ± 5.7 %, and control, 100.0 ± 4.3 %) (Fig. 6d).

High levels of ROS could exert oxidative stress and hinder an adequate tissue regeneration, which needs to be appropriately regulated to minimize the inflammatory response as well as promote a healthy tissue repair [18]. P/G@Ce, and P/G@IYCe groups showed negligible ROS-positive area. In contrast, control, P-control, and P/G groups exhibited significant amount of residual ROS (Fig. 6c). The ROS positive cell (P-cell) to cells ratio indicated the oxidative state of the wound microenvironment, which was found to be 84.3 ± 3.6 %, 84.3 ± 3.4 %, 77.8 ± 7.8 %, 34.8 ± 7.0 %, and 11.8 ± 4.0 % at the wound center, while 89.7 ± 1.9 %, 5.1 ± 1.4 %, 77.3 ± 2.5 %, 32.8 ± 5.3 %, and 25.7 ± 2.5 % at wound margin for control, P/G, P/G@IY, P/G@Ce, and P/G@IYCe groups at day 14, respectively (Fig. 6e and f). These results showed the significant potential of the P/G@IYCe to promote the regeneration of bacteria-infected wounds.

4. Discussion

The skin with structural integrity, serves as a protective barrier, which could detect external stimuli, regulate temperature, and prevent dehydration by retaining the moisture [24]. Nevertheless, multitudes of factors could disintegrate the structural integrity of the skin and adversely affect the normal structure and function of the skin, including trauma, disease, and surgical incisions [25]. Severe injuries, such as puncture wounds, lacerations, and burns may compromise intrinsic healing ability of the skin [22]. Moreover, once attacked by the microorganisms, chronic wounds including infectious wounds, venous ulcers or pressure ulcers may evolve, thereby further hamper skin repair [26]. Consequently, it is imperative to restore the structural integrity of the skin following skin injury [27,28]. While the administration of antibiotics is a viable option for the treatment of infectious wounds, an overuse of antibiotics may lead to antibiotics resistance [22]. Consequently, alternative strategies are necessary to avoid antibiotic resistance and overuse [28,29].

The P/G-based fibrous dressings manifest ECM-mimetic structure with high porosity and nano-scale pore size (Fig. 1b). Meanwhile these nanofiber dressings could isolate the wound site from the external environment and ensure permeability [30]. Moreover, owing to the porous structure of the fibrous dressings, these dressings may help incorporate and release therapeutics and biologics to promote the tissue repair (Fig. 1g). Antioxidative compounds, such as gallic acid and thymol can alleviate ROS albeit their rapid evaporation and instability [31]. On the other hand, ROS products can be catalyzed with enzymes, including catalase, which can directly scavenge the ROS [32]. Nonetheless, enzyme activity is susceptible to the different types of factors. Alternatively, NPs with catalytic enzyme-like activity, such as CeO_2 NPs and zinc oxide-copper sulphide (ZnO-CuS) NPs can be used to scavenge peroxides alongside additional biological functions [33,34]. Meanwhile, the IgY can be sustainably produced with high production yield owing to its simple collection method. The IgY has minimal side effects or disease resistance and therefore may be a viable approach for the treatment of infectious wounds (Fig. 3c) [14,35]. Consequently, we incorporated IgY and CeO_2 NPs into P/G dressings to afford P/G@IYCe to impart synergic antibacterial and ROS scavenging characteristics to the dressings (Fig. 7).

The P/G@IYCe dressing manifested good hemocompatibility and

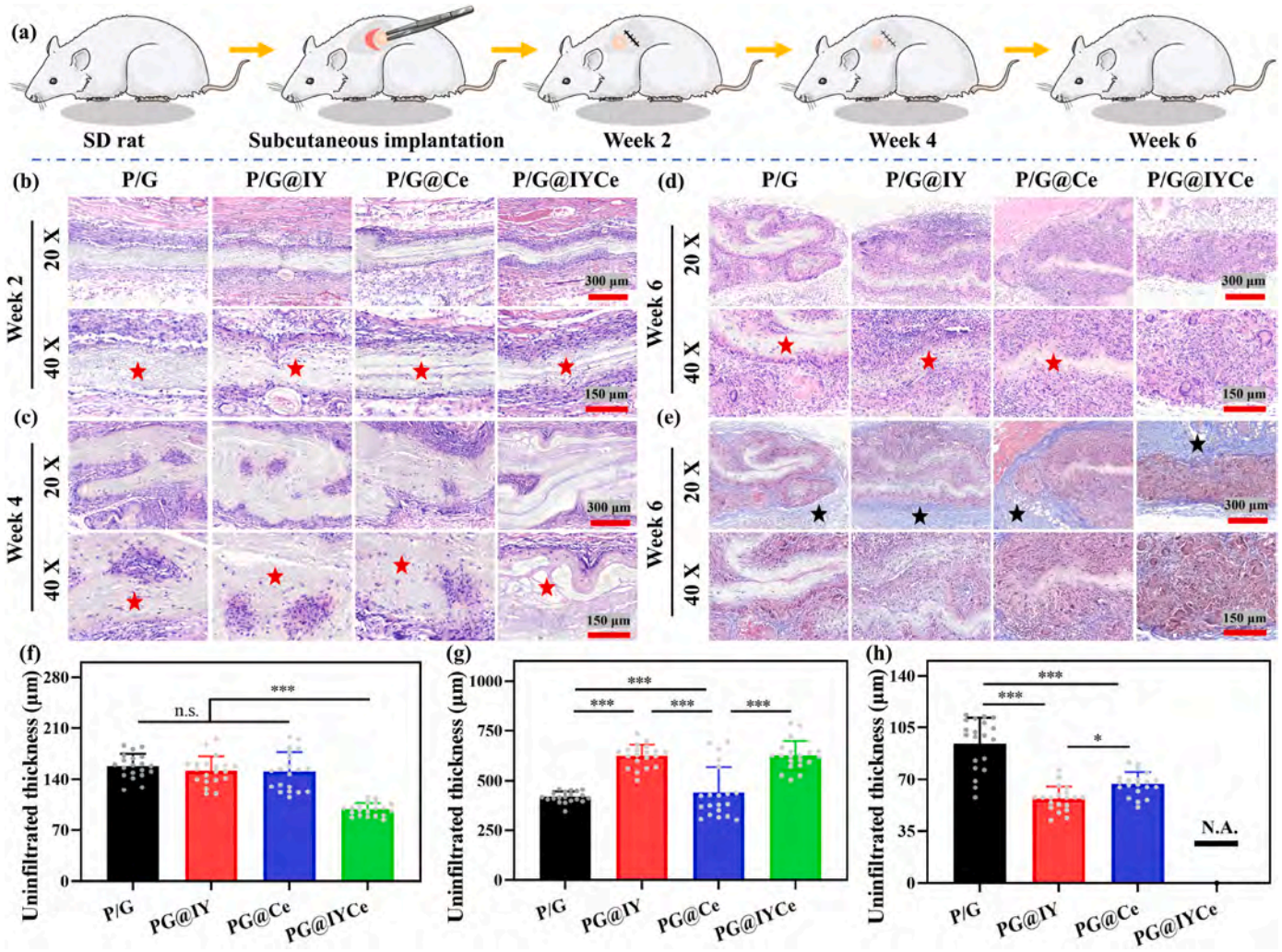

Fig. 4. Biocompatibility of electrospun fibers *in vivo*. (a) Schematic illustration of the biocompatibility of scaffolds in a subcutaneous implantation model *in vivo*. (b–c) H&E staining of scaffolds explanted at week 1 and 2 post-transplantation. H&E staining (d) and MT staining (e) of various scaffolds 3 weeks post-transplantation. (f–g) Quantitative analysis of the cellular infiltration into scaffolds at (f) 2 weeks, (g) 4 weeks, and (h) 6 weeks post-implantations. The red pentagrams point toward the scaffolds which were not infiltrated with the cells, while the black pentagrams point toward the regeneration of collagen tissues. (For interpretation of the references to colour in this figure legend, the reader is referred to the Web version of this article.)

biocompatibility *in vitro* alongside good biocompatibility *in vivo* (Fig. 2a–d, Fig. 4b–e). Compared with hydrogel materials, nanofibers exhibit a longer sustained release period, which may help avoid the ionic toxicity of the Ce [36]. Subcutaneous implantation assay manifested good biocompatibility of P/G@IYCe dressings alongside an appreciable degradation with the implantation (Fig. 4b–b). The rapid degradation of the dressings *in vivo* may be ascribed to: (i) The fast degradation of PLGA and Gel owing to their good hydrophilicity, and (ii) superior degradation of IgY and CeO_2 NPs [10]. While other polyesters, such as polycaprolactone (PCL) and polylactic acid (PLLA) show long-term degradation, PLGA possesses rapid degradation [31]. It is worthy to note that the degradation rate of the PLGA can be further controlled by varying the monomer ratio of the polymer. These dressings were further found to facilitate cell migration *in vitro* as assessed by using Transwell assay and scratching wound healing assay (Fig. 3a and b). These results indicated the P/G@IYCE could harness the reparative effect of the surrounding tissues towards the damaged site for a healthier wound tissue repair [22].

Skin repair involves multiple yet interacting phases e.g., cell proliferation and migration, inflammation resolution, angiogenesis, antimicrobial activity, etc. [4,20]. The healthy skin repair requires: *(i)* the synthesis of collagen tissues, *(ii)* elastic and reticular fibers, and (iii) ECM components, which involve multiple cellular events, such as cell proliferation, cell migration, angiogenesis, and granulation tissue formation [20]. The P/G@IYCe displayed distinct advantage to promote wound repair (Fig. 5b). Since IgY alone may be insufficient to meet the aforementioned criterion for a healthier skin repair, CeO_2 NPs were further loaded into dressings owing to their antibacterial, anti-inflammatory, anti-oxidative, and angiogenic properties, which may facilitate wound healing [37,38].

The severity of *S. aureus* infections and irrational use of antibiotics, such as penicillin in the clinical settings necessitates the development of antimicrobial agents with potent antimicrobial resistance [39]. Antibacterial assay revealed beneficial effect of IgY and CeO_2 NPs to suppress the growth of microorganisms, which may help overcome bacterial resistance problems currently being faced in the clinic (Fig. 3c). The IgY can treat various infectious diseases by various mechanisms, including agglutinating bacteria, constricted bacterial adhesion, suppression of virulence factors, toxin neutralization, opsonization and enzyme inactivation by the passive immunization, thereby further alleviating the biological functions of the pathogen [35,40]. Moreover, the IgY also offers other additional advantages for wound regeneration applications. Firstly, the IgY can be produced at a large-scale by employing eggs laid by immunizing hens along with the relative antigens [41]. IgY exhibits

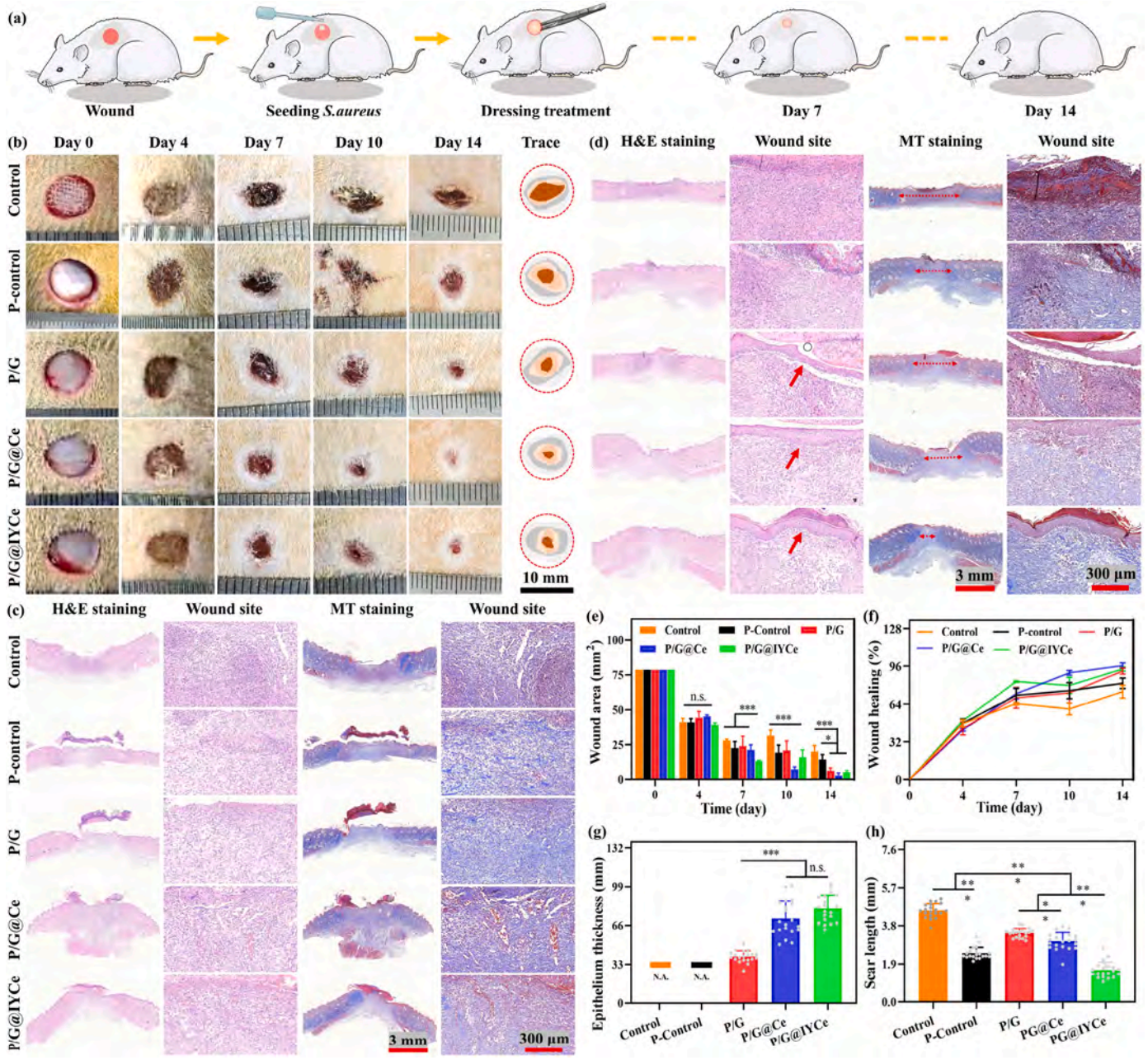

Fig. 5. Performance of membranes in a bacteria-infected full-thickness excisional defect model *in vivo*. (a) Schematic illustration showing the treatment of the wounds with various dressings for up to day 14. (b) Images of wound area and closure trace of wounds by day 14. H&E staining and MT staining of wound site at day 7 (c) and at day 14 (d). Residual wound area at different time point normalized with respect to day 0 (e). Percentage wound closure rate at day 14 (f). Epithelium thickness (g) and scar length (h) of regenerated skin.

high content of sialic acid, which can prolong its half-life; dry IgY can maintain its biological activity over the years [42]. The IgYs can also bind with the receptors of the complement activation system [43].

Meanwhile, the CeO_2 NPs may impart antibacterial activities by directly contacting with bacterial membranes and affecting the various function of certain ionic pumps to affect the exchange of transport between the bacterial cell and the environment, thereby restricting the bacterial growth [44]. The CeO_2 NPs could additionally furnish cerium ions to disrupt the flow of electrons as well as decrease the respiration and therefore may dislodge bacterial protein [7]. The cerium ions may either react with the thiol groups (-SH) or can be absorbed to the transporters and may hinder the transport of nutrients [7].

Thus, the IgY and CeO_2 NPs were used to prepare the P/G@IYCe dressing, which showed significant effect in term of promoting wound closure, suppressing residual bacteria at the injury site, improving epithelialization, and reconstruction, and limiting scar tissue formation (Fig. 5b and c). The P/G@Ce and P/G@IYCe groups showed significantly smaller number of ROS positive cells than that of the other groups, including P/G and P/G@IY putatively to the Ce; the latter has been shown to act as an anti-oxidative agent and scavenge multivarious ROS categories (e.g., superoxide anion radicle, nitric oxide radicle, etc.) (Fig. 6c). Interestingly, the cerium could maintain either in a reduced (Ce^{+3}) or a completely oxidized (Ce^{+4}) form, which could change its electronic configuration and scavenge ROS [45]. The CeO_2 NPs with a high concentration of cerium ions (Ce^{3+}) may display a stable anti-oxidative function to eliminate ROS [7].

Angiogenesis involves the production *de novo* capillaries from pre-existing vessels to generate a complex blood vessel network, which

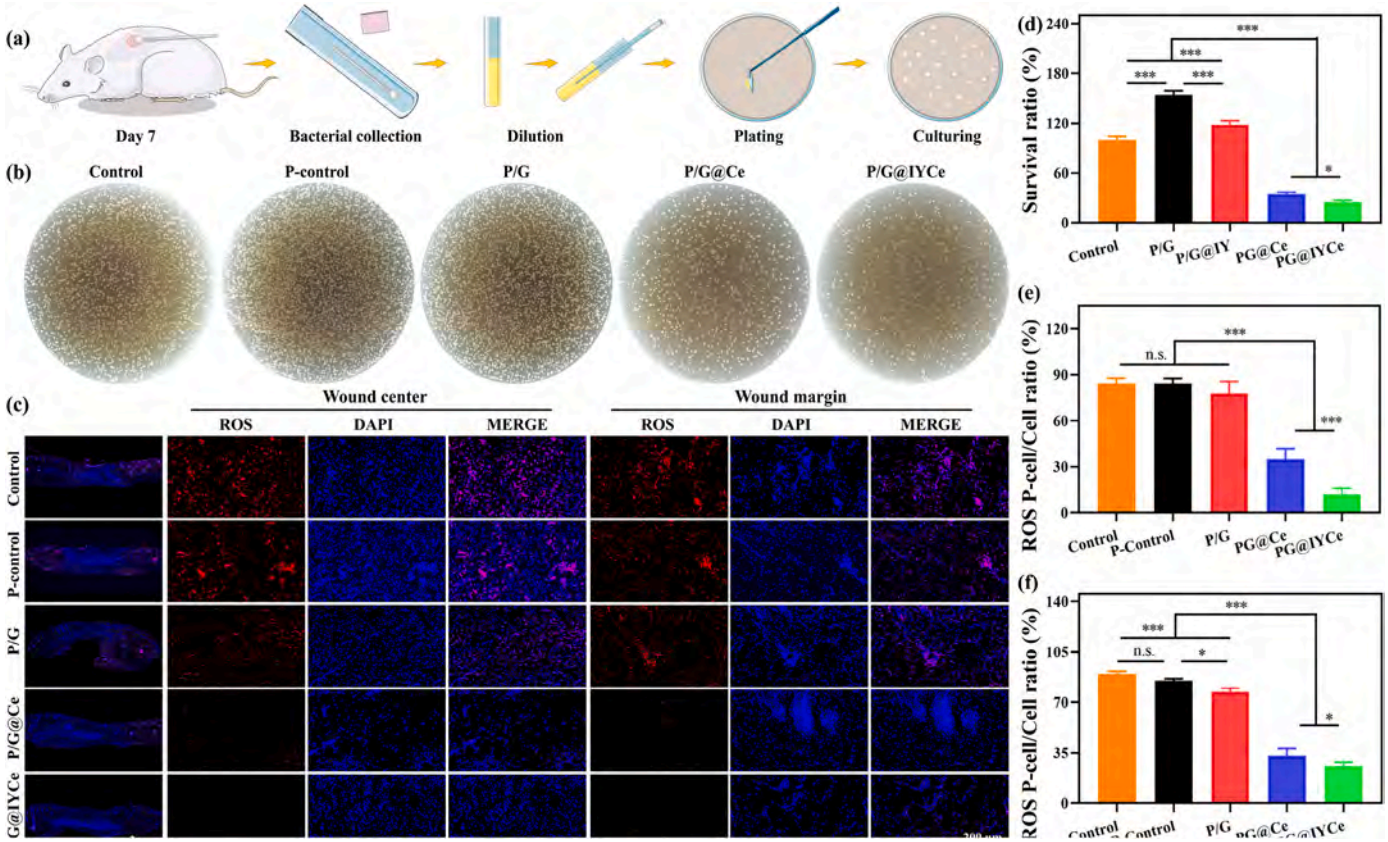

Fig. 6. (a) Schematic illustration of antibacterial analysis of the wounds. (b) Growth of *S. aureus* collected from residual bacteria at wound site by day 7. (c) ROS IF staining of wound site at day 14. (d) Survival ratio of residual bacteria at wound site by day 7. The ROS positive cell (P-cell) to cells ratio at the wound center (e) and wound margin (f).

involves cell proliferation, cell migration, and endothelial network formation of endothelial cells [20]. *De novo* blood vessels may facilitate oxygen diffusion and nutrient transport, thereby promoting the tissue repair [20]. The CeO_2 NPs could promote angiogenesis by adjusting the intracellular oxygen environment, and induce the translocation of hypoxia-inducing factor 1α (HIF-1α) to the nucleus, further stimulates the expression of various proteins referring to angiogenesis [36]. Taken together, P/G@IYCe dressings may possess broad implications for skin repair.

Despite these encouraging results, these are still several limitations for the long-term clinical translation of these membranes. Firstly, a thorough investigation of the skin repair mechanism, such as gene and protein expression analysis need to be carried out. Secondly, it is necessary to optimize the animal model by using of rubber bands in wound site, which could effetely avoid the error of the regenerative effect caused by skin contraction in the regeneration process. Thirdly, based on the multifunctional therapeutic effect of IgY and CeO_2 NPs, evaluation of membranes in the large animal models and other bio-related disciplines may have considerable significance for the future investigations. Finally, we did not carry out the long-term cytotoxicity or immunological response to the degradation byproducts, which would be important to further qualify the materials for clinical applications.

5. Conclusion

The oxidative stress typically occurs during the initial phases of tissue repair post-injury; overproduction of oxidative stress may pose deleterious effect on different cell types including endothelial cells and impair the formation of neo-vessels and tissues. We co-loaded IgY and CeO_2 NPs to impart multifunctionality to the dressings, such as ROS scavenging, anti-inflammatory response, and anti-bacterial response. The P/G@IYCe dressing showed potential application for rapid wound closure (around 73.3 % at day 14), enhanced re-epithelialization, granulation tissue formation, inflammation resolution, and anti-bacterial behaviors (24.6 % bacteria survival ratio) in *S. aureus* infected wound.

CRediT authorship contribution statement

Xinyuan Zhao: Writing – original draft, Software, Investigation, Formal analysis, Conceptualization. **Changwen Weng:** Software, Investigation, Data curation. **Hao Feng:** Visualization, Investigation. **Muhammad Shafiq:** Writing – review & editing, Supervision, Project administration, Funding acquisition. **Xinyi Wang:** Software, Formal analysis, Data curation. **Lei Liu:** Validation, Formal analysis. **Lu Han:** Software, Data curation. **Mohamed EL-Newehy:** Funding acquisition, Conceptualization. **Meera Moydeen Abdulhameed:** Methodology, Funding acquisition. **Zhengchao Yuan:** Writing – original draft, Supervision, Conceptualization. **Xiumei Mo:** Writing – review & editing, Visualization, Supervision, Funding acquisition. **Yanbiao Wang:** Writing – review & editing, Supervision, Funding acquisition.

Declaration of interests

The authors declare that they have no known competing financial interests or personal relationships that could have appeared to influence the work reported in this paper. Thanks for http://www.home-for-researchers.com creating the Fig.7.

Declaration of competing interest

The authors declare that they have no known competing financial

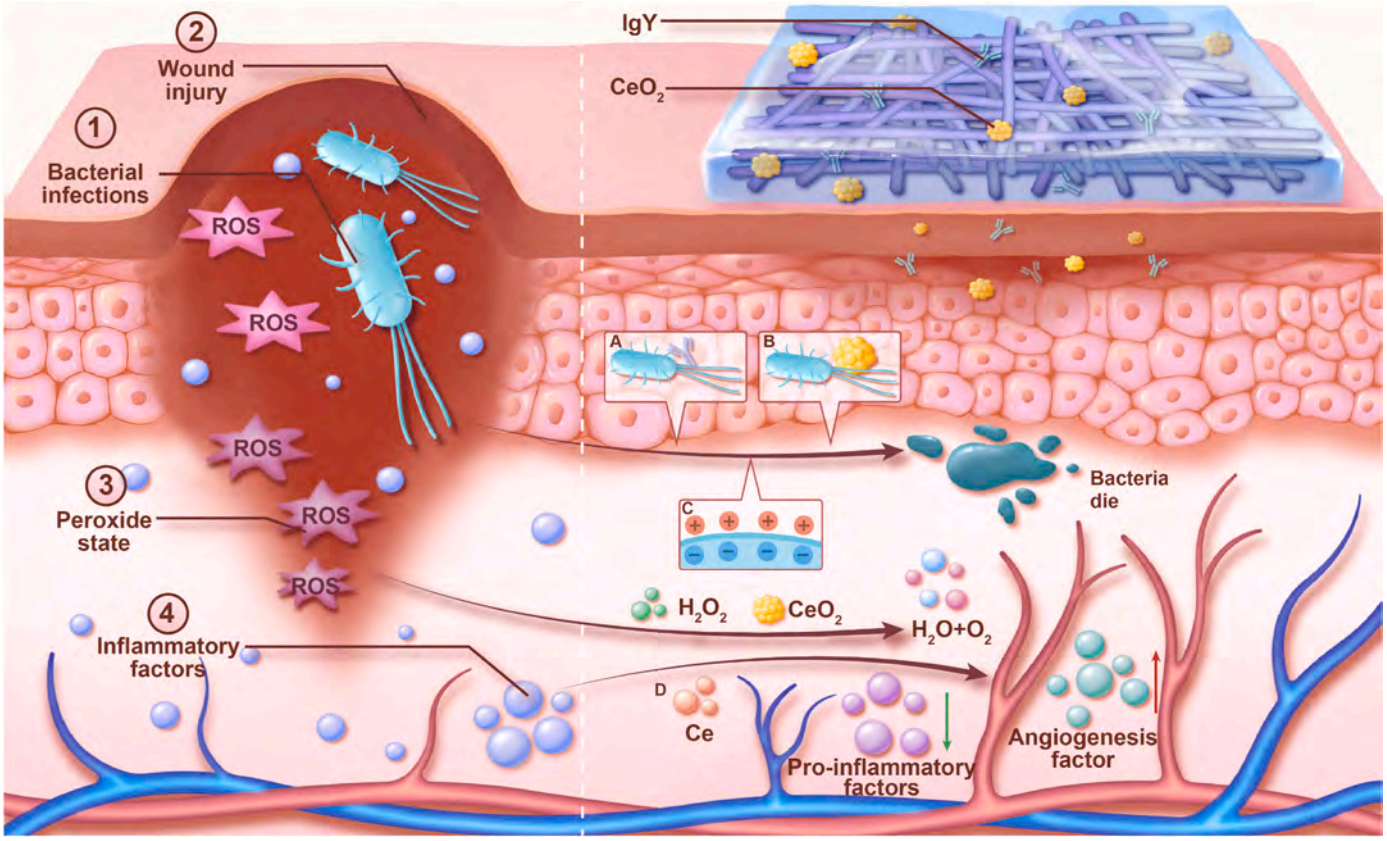

Fig. 7. Schematic illustration of the mechanism of improved wound healing by PG@IYCe dressings.

interests or personal relationships that could have appeared to influence the work reported in this paper.

Acknowledgements

This project was supported by the Fundamental Research Funds for the Central Universities and Graduate Student Innovation Fund of Donghua University (CUSF-DH-D-2024040), Science and Technology Commission of Shanghai Municipality, China (20DZ2254900), Sino German Science Foundation Research Exchange Center, China (M – 0263), and China Education Association for International Exchange (2022181). This project was also supported by Researchers Supporting Project Number (RSP2025R65), King Saud University, Riyadh, Saudi Arabia.

Appendix A. Supplementary data

Supplementary data to this article can be found online at https://doi.org/10.1016/j.mtbio.2024.101408.

Data availability

Data will be made available on request.

References

[1] H. Wang, Q. Zhong, J. Lin, Egg yolk antibody for passive immunization: status, challenges, and prospects, J. Agric. Food Chem. 71 (2023) 5053–5061.
[2] J. Song, I.H. Chowdhury, S. Choudhuri, A.E.I. Ayadi, L.E. Rios, S.E. Wolf, J. C. Wenke, N.J. Garg, Acute muscle mass loss was alleviated with HMGB1 neutralizing antibody treatment in severe burned rats, Sci. Rep. 13 (2023) 10250.
[3] J. Shan, J. Che, C. Song, Y. Zhao, Emerging antibacterial nanozymes for wound healing, Smart Med. 2 (2023) e20220025.
[4] Y. Xu, Q. Saiding, X. Zhou, J. Wang, W. Cui, X. Chen, Electrospun fiber-based immune engineering in regenerative medicine, Smart Med 3 (2024) e20230034.
[5] A.L. Pignet, A. Hecker, T. Voljc, M. Carnieletto, N. Watzinger, L.P. Kamolz, The use of acellular fish skin grafts in burns and complex trauma wounds: a systematic review of clinical data, Plast. Aesthetic Res. 11 (2024) 40.
[6] X. Fu, J. Wang, D. Qian, L. Xi, L. Chen, Y. Du, W. Cui, Y. Wang, Oxygen atom-concentrating short fibrous sponge regulates cellular respiration for wound healing, Adv. Fiber Mater. 5 (2023) 1773–1787.
[7] H. Nosrati, M. Heydari, M. Khodaei, Cerium oxide nanoparticles: synthesis methods and applications in wound healing, Mater. Today Bio. 23 (2023) 100823.
[8] C. Li, B. Yi, Q. Xu, J. Ma, L. Yuan, Y. Liu, W. Liu, Z. Zhou, X. Ning, J. Zhang, F. Yang, S. Wang, Q. Shi, Q. Zhou, Z. Wang, ADSCC-CM-induced keratin hydrogel-based bioactive microneedle patch containing triamcinolone acetonide for the treatment of pathological scar, Adv. Funct. Mater. 34 (2024) 2400457.
[9] M. Ranjbar, B. Behrouz, F. Norouzi, S.L. Mousavi Gargari, Anti-PcrV IgY antibodies protect against Pseudomonas aeruginosa infection in both acute pneumonia and burn wound models, Mol. Immunol. 116 (2019) 98–105.
[10] L. Sun, Z. Chen, L. Guo, Z. Geng, X. Chen, Proteomic analysis of egg yolk proteins during embryonic development in wanxi white goose, J. Agric. Food Chem. 72 (2024) 5212–5221.
[11] L. Zhang, L. Lin, Z. Qin, A review on the application of chicken immunoglobulin Y in aquaculture, Rev. Aquac. 16 (2024) 536–551.
[12] K. Thomsen, L. Christophersen, T. Bjarnsholt, P. Jensen, C. Moser, N. Høiby, Anti-Pseudomonas aeruginosa IgY antibodies augment bacterial clearance in a murine pneumonia model, J. Cyst. Fibros. 15 (2016) 171–178.
[13] B. Narayan Biswal, S. Narayan Das, B. Kumar Das, R. Rath, Alteration of cellular metabolism in cancer cells and its therapeutic, J. Oral Maxillofac. Pathol. 21 (2017) 244–251.
[14] A.S. Dousari, S.S. Hosseininasab, M.R. Akbarizadeh, M. Naderifar, A. Mahdavi, N. Satarzadeh, A review on immunoglobulin Y (IgY) conjugated with metal nanoparticles and biomedical uses, Bioprocess Biosyst. Eng. 46 (2023) 1533–1538.
[15] E.P.V. Pereira, M.F. van Tilburg, E.O.P.T. Florean, M.I.F. Guedes, Egg yolk antibodies (IgY)and their applications in human and veterinary health: a review, Int. Immunopharmacol. 73 (2019) 293–303.
[16] X. Fu, J. Wang, D. Qian, Z. Chen, L. Chen, W. Cui, Y. Wang, Living electrospun short fibrous sponge via engineered nanofat for wound healing, Adv. Fiber Mater. 5 (2023) 979–993.
[17] F. Kavanagh, W. Rozen, I. Seth, R. Cuomo, Exploring the efficacy of negative pressure wound therapy in the management of mycobacterium ulcerans wounds: a comprehensive literature review, Plast. Aesthetic Res. 11 (2024) 43.
[18] Z. Yuan, M. Shafiq, H. Zheng, L. Zhang, Z. Wang, X. Yu, J. Song, B. Sun, M. El-newehy, H. El-hamshary, Multi-functional fibrous dressings for infectious injury treatment with anti-adhesion wound healing, Mater. Des. 235 (2023) 112459.

[19] G. Kaur, G. Narayanan, D. Garg, A. Sachdev, I. Matai, Biomaterials-based regenerative strategies for skin tissue wound healing, ACS Appl. Bio Mater. 5 (2022) 2069–2106.
[20] Z. Yuan, L. Zhang, S. Jiang, M. Sha, Y. Cai, Y. Chen, J. Song, X. Yu, H. Ijima, Y. Xu, X. Mo, Anti-inflammatory, antibacterial, and antioxidative bioactive glass-based nanofibrous dressing enables scarless wound healing, Smart Mater. Med. 4 (2023) 407–426.
[21] W. Nie, E.J. Marrotte, R. Xie, H.G. Machens, A.F. Schilling, Y. Shen, M. Seeds, A. Atala, X. Dai, Towards scarless repair: MMP-2 responsive drug releasing nanofibrous mat restores homeostasis via fibroblasts' activation, Compos. Part B Eng. 291 (2024) 111972.
[22] Z. Yuan, Y. Zhao, M. Shafiq, J. Song, J. Hou, Y. Liang, X. Yu, Multi - functional fibrous dressings for burn injury treatment with pain and swelling relief and scarless wound healing, Adv. Fiber Mater. 5 (2023) 1963–1985.
[23] Y. Li, S. Liu, J. Zhang, Y. Wang, H. Lu, Y. Zhang, G. Song, F. Niu, Y. Shen, A. C. Midgley, W. Li, D. Kong, M. Zhu, Elastic porous microspheres/extracellular matrix hydrogel injectable composites releasing dual bio-factors enable tissue regeneration, Nat. Commun. 15 (2024) 1377.
[24] J. Wang, J. Lin, L. Chen, L. Deng, W. Cui, Endogenous electric-field-coupled electrospun short fiber via collecting wound exudation, Adv. Mater. 34 (2022) 2018325.
[25] X. Han, S. Chen, Z. Cai, Y. Zhu, W. Yi, M. Guan, B. Liao, Y. Zhang, J. Shen, W. Cui, D. Bai, A diagnostic and therapeutic hydrogel to promote vascularization via blood sugar reduction for wound healing, Adv. Funct. Mater. 33 (2023) 2213008.
[26] G. Cai, Z. Yuan, X. Wang, S. Wu, S. Zhou, Z. Lei, Grafts : salutatory effect of the BVLD and EGCG-Cu to promote hemocompatibility and nitric oxide production for in situ blood vessel regeneration, Chem. Eng. J. 500 (2024) 156555.
[27] M. Huang, Z. Yuan, G. Fu, J. Dong, Y. Sun, W. Wang, M. Shafiq, H. Cao, X. Mo, J. Chen, An injectable antibacterial wet-adhesive for meniscal cartilage regeneration via immune homeostasis mediated by SMSC-derived extracellular vesicles, Compos. Part B Eng. 291 (2024) 111970.
[28] C. Hong, H. Chung, G. Lee, C. Kim, D. Kim, S.J. Oh, S.H. Kim, K. Lee, Hydrogel/nanofiber composite wound dressing optimized for skin layer regeneration through the mechanotransduction-based microcellular environment, ACS Appl. Bio Mater. 6 (2023) 1774–1786.
[29] S. Mcloughlin, A.R. Mckenna, J.P. Fisher, Fabrication strategies for engineered thin membranous tissues, ACS Appl. Bio Mater. 6 (2023) 2546–2561.
[30] H. Li, X. Xu, L. Wu, X. Chen, H. Akhter, Y. Wang, P. Song, X. Liao, Z. Zhang, Z. Li, C. Zhou, Y. Cen, H. Ai, X. Zhang, Recent progress and clinical applications of advanced biomaterials in cosmetic surgery, Regen. Biomater. 10 (2023) rbad005.
[31] X. Haixia, Z. Peng, L. Jiezhao, G. Huiling, C. Xie, W. Yihan, J. Yanglei, J. Li, C. Wang, X. Wenning, Z. Lixin, C. Liu, 3D-printed magnesium peroxide-incorporated scaffolds with sustained oxygen release and enhanced photothermal performance for osteosarcoma multimodal treatments, ACS Appl. Mater. Interfaces 16 (2024) 9626–9639.
[32] S. Liu, Y. Sun, J. Ye, C. Li, Q. Wang, M. Liu, Y. Cui, C. Wang, G. Jin, Y. Fu, J. Xu, X. Liang, Targeted delivery of active sites by oxygen vacancy-engineered bimetal silicate nanozymes for intratumoral aggregation-potentiated catalytic therapy, ACS Nano 18 (2) (2024) 1516–1530.
[33] V.A. Petrova, I.V. Gofman, N.V. Dubashynskaya, A.S. Golovkin, A.I. Mishanin, E. M. Ivan'kova, Y.A. Skorik, Chitosan composites with bacterial cellulose nanofibers doped with nanosized cerium oxide: characterization and cytocompatibility evaluation, Int. J. Mol. Sci. 6 (2023) 5415.
[34] Y. Sun, W. Zhang, Z. Luo, C. Zhu, Y. Zhang, Z. Shu, C. Shen, X. Yao, Y. Wang, X. Wang, ZnO-CuS/F127 hydrogels with multienzyme properties for implant-related infection therapy by inhibiting bacterial arginine biosynthesis and promoting tissue repair, Adv. Funct. Mater. (2024) 2415778.
[35] T.S. Ahmadi, B. Behrouz, S.L. Mousavi Gargari, Polyclonal anti-whole cell IgY passive immunotherapy shields against P. aeruginosa-induced acute pneumonia and burn wound infections in murine models, Sci. Rep. 14 (2024) 405.
[36] Z. Zheng, X. Yang, M. Fang, J. Tian, S. Zhang, L. Lu, C. Zhou, C. Xu, Y. Qi, L. Li, Photothermal effective CeO_2NPs combined in thermosensitive hydrogels with enhanced antibacterial, antioxidant and vascularization performance to accelerate infected diabetic wound healing, Regen. Biomater. 10 (2023) rbad072.
[37] L. Xiao, H. Liu, H. Huang, S. Wu, L. Xue, Z. Geng, L. Cai, F. Yan, 3D nanofiber scaffolds from 2D electrospun membranes boost cell penetration and positive host response for regenerative medicine, J. Nanobiotechnology. 22 (2024) 322.
[38] A.H. Taghvaei, F. Danaeifar, C. Gammer, J. Eckert, S. Khosravimelal, M. Gholipourmalekabadi, Synthesis and characterization of novel mesoporous strontium-modified bioactive glass nanospheres for bone tissue engineering applications, Microporous Mesoporous Mater. 294 (2020) 109889.
[39] R.K. Kota, P.N. Reddy, K. Sreerama, Application of IgY antibodies against staphylococcal protein A (SpA) of staphylococcus aureus for detection and prophylactic functions, Appl. Microbiol. Biotechnol. 104 (2020) 9387–9398.
[40] S.A. El-Kafrawy, A.T. Abbas, C. Oelkrug, M. Tahoon, S. Ezzat, A. Zumla, E.I. Azhar, IgY antibodies: the promising potential to overcome antibiotic resistance, Front. Immunol. 14 (2023) 1065353.
[41] K. Brumfield, H. Seo, N. Idegwu, C. Artman, L. Gonyar, J. Nataro, W. Zhang, D. Sack, J. Geyer, J. Goepp, Feasibility of avian antibodies as prophylaxis against enterotoxigenic escherichia coli colonization, Front. Immunol. 13 (2022) 1011200.
[42] X. Zhou, S. Ma, Anti-lipopolysaccharide egg yolk antibodies enhance the phagocytosis of mammalian phagocytes, Biol. Open 7 (2018) bio032821.
[43] E. Nilsson, A. Larsson, H.V. Olesen, P.E. Wejåker, H. Kollberg, Good effect of IgY against Pseudomonas aeruginosa infections in cystic fibrosis patients, Pediatr. Pulmonol. 43 (2008) 892–899.
[44] S. Selvaraj, A. Chauhan, A. Radhakrishnan, G. Rana, V. Dutta, K.M. Batoo, S. Ghotakar, Cerium oxide nanoparticles and their polymeric composites: advancements in biomedical applications, J. Inorg. Organomet. Polym. Mater. 34 (2024) 5691–5717.
[45] N. Melnikova, D. Malygina, V. Korokin, H. Al-Azzawi, D. Zdorova, E. Mokshin, E. Liyaskina, I. Kurgaeva, V. Revin, Synthesis of cerium oxide nanoparticles in a bacterial nanocellulose matrix and the study of their oxidizing and reducing properties, Molecules 28 (2023) 2604.